C1 CAGE detects transcription start sites and enhancer activity at single-cell resolution

Tsukasa Kouno[1*], Jonathan Moody[1*], Andrew Kwon[1*], Youtaro Shibayama[1], Sachi Kato[1], Yi Huang[1,2], Michael Böttcher[1], Efthymios Motakis[1,3], Mickaël Mendez[1,4], Jessica Severin[1], Joachim Luginbühl[1], Imad Abugessaisa[1], Akira Hasegawa[1], Satoshi Takizawa[1], Takahiro Arakawa[1], Masaaki Furuno[1], Naveen Ramalingam[5], Jay West[5], Harukazu Suzuki[1], Takeya Kasukawa[1], Timo Lassmann[1,6], Chung-Chau Hon[1], Erik Arner[1], Piero Carninci[1], Charles Plessy[1#] and Jay W Shin[1#]

1 RIKEN Center for Integrative Medical Sciences (IMS), 1-7-22 Suehiro-cho, Tsurumi-ku, Yokohama, 230-0045 Japan
2 Present address: ACT Genomics Co., LTD., 3F., No.345, Xinhu 2nd Rd., Neihu Dist., Taipei City 114, Taiwan
3 Present address: Yong Loo Lin School of Medicine MD6, #08-01, 14 Medical Drive, National University of Singapore, Singapore 117599
4 Present address: Princess Margaret Cancer Research Tower 11-401, 101 College Street, Toronto, ON M5G 1L7 Canada
5 Single-Cell Research and Development, 7000 Shoreline Court, Suite 100, South San Francisco, California, USA 94080.
6 Present address: Telethon Kids Institute, The University of Western Australia, Subiaco, Australia

(*) Authors contributed equally
(#) Corresponding authors: plessy@riken.jp, jay.shin@riken.jp

Abstract

Single-cell transcriptomic profiling is a powerful tool to explore cellular heterogeneity. However, most of these methods focus on the 3'-end of polyadenylated transcripts and provide only a partial view of the transcriptome. We introduce C1 CAGE, a method for the detection of transcript 5'-ends with an original sample multiplexing strategy in the C1™ microfluidic system. We first quantified the performance of C1 CAGE and found it as accurate and sensitive as other methods in C1 system. We then used it to profile promoter and enhancer activities in the cellular response to TGF-β of lung cancer cells and discovered subpopulations of cells differing in their response. We also describe enhancer RNA dynamics revealing transcriptional bursts in subsets of cells with transcripts arising from either strand within a single-cell in a mutually exclusive manner, which was validated using single molecule fluorescence in-situ hybridization.

Introduction

Single-cell transcriptomic profiling can be used to uncover the dynamics of cellular states and gene regulatory networks within a cell population(Trapnell, 2015; Wagner, Regev and Yosef, 2016). Most available single-cell methods capture the 3'-end of transcripts and are unable to identify where transcription initiates. Instead, capturing the 5'-end of transcripts allows the identification of transcription start sites (TSS) and thus the inference of the activities of their regulatory elements. Cap analysis gene expression (CAGE), which captures the 5'-end of transcripts, is a powerful tool to identify TSS at single nucleotide resolution(Shiraki *et al.*, 2003; Carninci *et al.*, 2006). Using this technique, the FANTOM consortium has built an atlas of TSS across major human cell-types and tissues(Forrest *et al.*, 2014), analysis of which has led to the identification of promoters as well as enhancers in the human genome(Andersson *et al.*, 2014; Hon *et al.*, 2017). Enhancers have been implicated in a variety of biological processes(Lam *et al.*, 2014; Li, Notani and Rosenfeld, 2016), including the initial activation of responses to stimuli(Arner *et al.*, 2015) and chromatin remodeling for transcriptional activation(Mousavi *et al.*, 2013). In addition, over 60% of the fine-mapped causal noncoding variants in autoimmune disease lay within immune-cell enhancers (Farh *et al.*, 2015), suggesting the relevance of enhancers in pathogenesis of complex diseases. Enhancers have been identified by the presence of balanced bidirectional transcription producing enhancer RNAs (eRNAs), which are generally short, unstable and non-polyadenylated (non-polyA)(Andersson *et al.*, 2014). Single molecule fluorescence *in situ* hybridization (smFISH) studies have suggested that eRNAs are induced with similar kinetics to their target mRNAs but that co-expression at individual alleles was infrequent(Rahman *et al.*, 2016). However, the majority of enhancer studies have been conducted using bulk populations of cells meaning that the dynamics of how multiple enhancers combine to influence gene expression remains unknown.

The majority of single-cell transcriptomic profiling methods(Picelli, 2017) rely on oligo-dT priming during reverse transcription, which does not capture non-polyA RNAs transcripts (e.g. eRNAs). The recently developed RamDA-seq(Hayashi *et al.*, 2018) method uses random priming to capture the full-length non-polyA transcripts including eRNAs. However, this method is not strand-specific and unable to pinpoint transcript 5'-ends; thus, it cannot detect the bidirectionality of eRNA transcription and cannot confidently distinguish reads derived from the primary transcripts of their host gene (i.e. intronic eRNAs). Methods are typically implemented for a specific single-cell handling platform (e.g. microwell, microfluidics or droplet-based

platforms)(Picelli, 2017), because each platform imposes strong design constraints on the critical steps of cell lysis and nucleic acid handling. The proprietary C1™ Single-Cell Auto Prep System (Fluidigm) uses disposable integrated fluidic circuits (IFCs) and provides a registry of publicly available single-cell transcriptomics methods (Supplementary Table 1), which can be customized. Previously, we introduced nanoCAGE(Plessy *et al.*, 2010), a method requiring only nanograms of total RNA as start material, based on a template switch mechanism combined with random priming to capture the 5'-ends of transcripts independent of polyA tails in a strand-specific manner. Here we develop C1 CAGE, a modified version of nanoCAGE customized to the C1 system to capture the 5'-ends of transcripts at single-cell resolution.

Current single-cell methods are usually limited in the number of samples that can be multiplexed within the same run. Thus, experimental designs requiring multiple replicates and different conditions are prone to batch effects, confounding biological information with the technical variation of each experiment(Tung *et al.*, 2017). To mitigate batch effects, we took advantage of the transparency of the C1 system to encode multiple cells perturbation states in a single run by fluorescent labeling and imaging.

We apply this method to investigate the response to TGF-β in A549 cells, an adenocarcinomic human alveolar basal epithelial cell line. TGF-β signaling plays a key role in embryonic development, cancer progression, host tumor interactions and driving epithelial-to-mesenchymal transition (EMT)(Massagué, 2008; Ikushima and Miyazono, 2010). We examine the response to TGF-β in A549 cells to uncover dynamically regulated promoters and enhancers at single-cell resolution. We observed an asynchronous cellular response to TGF-β in sub-populations of cells. We also investigated the dynamics of enhancer transcription at single-cell resolution with validation by smFISH. Our results suggest transcriptional bursting of enhancers as reflected by high expression of eRNAs in a few cells. Also, while in pooled cells enhancers show bidirectional transcription, within single-cells transcription at enhancers is generally unidirectional—i.e. transcription on the two strands seems to be mutually exclusive.

98 # Results

99 **Development of C1 CAGE**

100 We developed the C1 CAGE method, based on nanoCAGE(Plessy *et al.*, 2010), C1 STRT
101 Seq(Islam *et al.*, 2014) and C1 RNA-seq(Wu *et al.*, 2014), implementing reverse transcription
102 with random hexamers followed by template switching and pre-amplification (Figure 1a). The
103 cDNA is tagmented and the 5'-end of cDNA is specifically amplified by index PCR. The resulting
104 library is sequenced from both ends, with the forward reads identifying the 5'-end of the
105 transcript at single nucleotide resolution and the reverse read identifying downstream regions of
106 the matching transcript.
107
108 To assess the specificity of 5'-end capture, we prepared libraries of A549 cells in the presence
109 of synthetic "spike-in" RNAs, a set of 92 exogenous control transcripts with defined abundances
110 developed by the External RNA Controls Consortium (ERCC)(Munro *et al.*, 2014). We analyzed
111 the positions of forward reads on these spike-ins and found that ~80% of their 5'-ends align to
112 the first base (Figure 1b), supporting the specificity of 5'-end capture in C1 CAGE. Of the
113 remaining reads, about half of them can be explained by "strand-invasion" events, which are
114 artefacts arising from interruption of first strand synthesis due to complementarity with the
115 template switching oligonucleotide and can be identified based on the upstream sequence of
116 the read(Tang *et al.*, 2013). Next, we assessed the quantification accuracy and molecular
117 detection limit(Svensson *et al.*, 2017). For quantification accuracy, measured as the Pearson
118 correlation between the input spike-in amounts and the observed read counts, C1 CAGE
119 displayed a median of 0.79, slightly higher (Welch Two Sample t-test, two-sided, $p < 0.0001$)
120 than C1 STRT Seq (median of 0.74, Figure 1c). For detection limit, measured as the median
121 number of spike-in molecules required to give a 50% chance of detection, C1 CAGE displayed a
122 median of 22, which is significantly more sensitive (Welch Two Sample t-test, two-sided, $p <$
123 $2.2e-16$) compared with C1 STRT Seq (median of 146, Figure 1d). Finally, we assessed the
124 ability of C1 CAGE to detect differential expression by comparing libraries prepared using two
125 reference mixtures of spike-ins with fixed ratios of input amounts at 4, 1, 2/3 and 1/2 fold
126 difference. Fitting a linear model we find an R-squared value of 87%(Figure 1e). These results
127 demonstrate that C1 CAGE specifically captures the 5'-end of transcripts, has quantification
128 accuracy and detection sensitivity comparable to other C1-system methods, and reliably detects
129 differential expression with high accuracy.

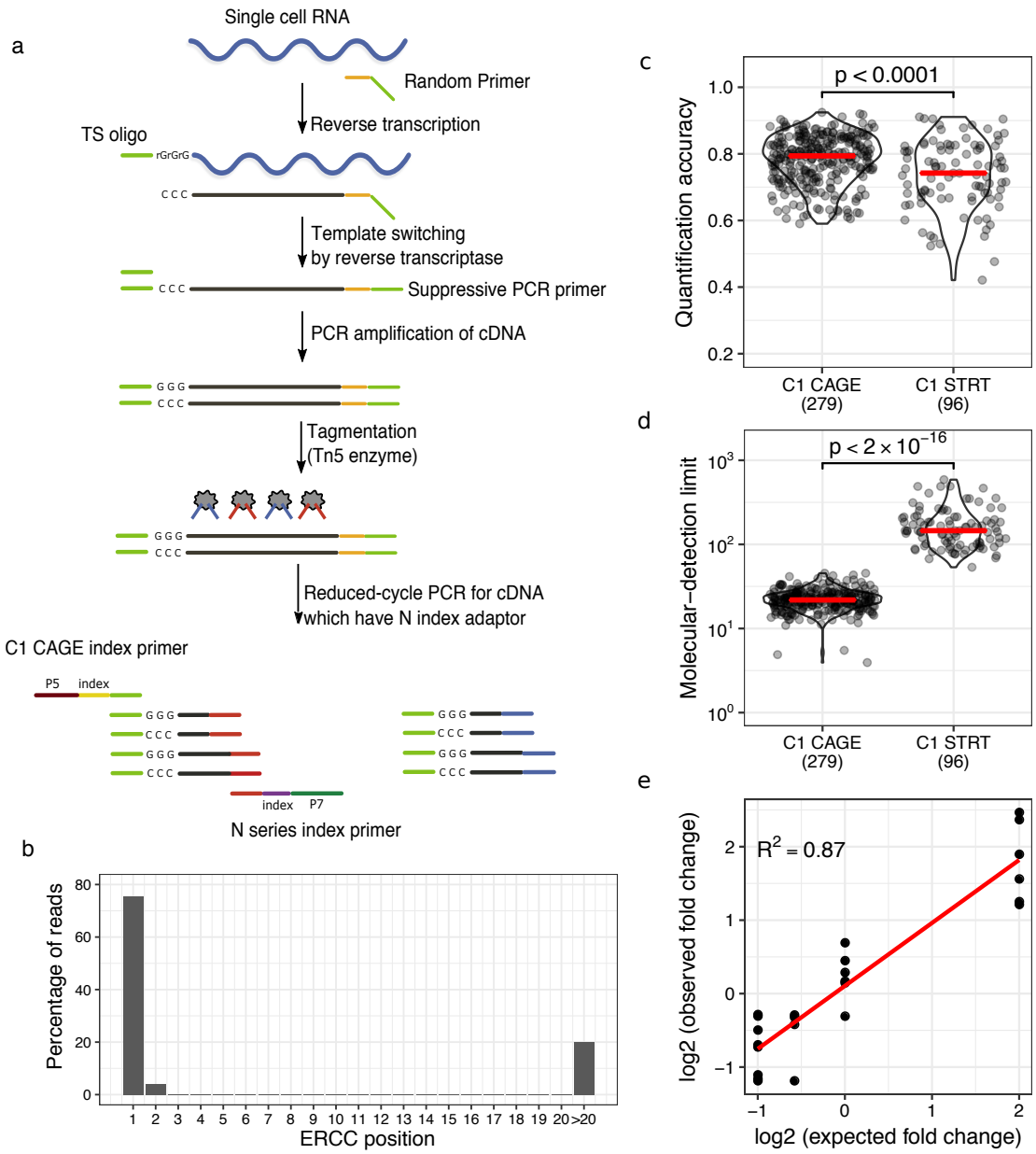

Figure 1: C1 CAGE method and performance

(a) Schematic of the C1 CAGE method. Tn5 enzymes are loaded with two different adaptors: N (red) and S (blue). P5, P7: Illumina sequencing adaptors. (b) Percentage of reads aligning to the 5'-end of ERCC spike-ins by nucleotide position. (c, d) Comparison between C1 CAGE and C1 STRT Seq (data from doi:10.1038/nmeth.4220). Red bars show median values. p-values from Welch two-sided Two Sample t-test shown. (c) Pearson correlation between expected and observed ERCC spike-in molecules. (d) The number of ERCC spike-in molecules required for a 50 % chance of detection. (e) Observed and expected fold-change ratios between ERCC mix1 and mix2. Linear regression line (red) and R-squared value shown.

140 **Color multiplexing**

141 Taking advantage of the imaging capacities of the C1 system, we devised a strategy to
142 multiplex samples within the same C1 CAGE replicate, by labelling cells with different Calcein
143 AM dyes to encode sample information and monitor cell viability at the same time. Based on this
144 approach, we multiplexed samples of A549 cells stimulated with TGF-β in a time-course at three
145 time-points (0, 6, and 24 h, in triplicates) by permuting the Calcein AM dyes for each time point
146 in each replicate (Figure 2a). The three C1 CAGE replicates were sequenced to a median depth
147 of 2.4 million raw read pairs per cell. Analyzing the genomic distribution of forward read 5'-ends
148 per replicate, a mean of 34% and 0.7% of reads were aligned to promoter and enhancer CAGE
149 clusters, respectively (Figure 2b). Subsampling analysis demonstrates the number of CAGE
150 clusters detected in most single-cells are saturated at the current sequencing depths, with a
151 median of 2,788 CAGE clusters detected per cell (Figure 2c). To demultiplex time points, we
152 localized the cells in their capture chambers on the IFCs and quantified their fluorescence in the
153 red and green channels, identifying 40, 41 and 70 cells for time points 0, 6 and 24 h,
154 respectively. Following the scran pipeline(Lun, McCarthy and Marioni, 2016) we removed 15
155 unreliable cells, arriving at the final set of 136 high quality cells. Initially, we observed a strong
156 batch effect with principal components analysis (PCA), where cells cluster by replicate (Figure
157 S1a). However, our experimental design ensured that each replicate contained cells for each
158 time point, allowing us to correct for this batch effect using linear modelling. After batch
159 correction cells were clustered by time points rather than by replicate (Figure S1b). After
160 removing low abundance CAGE clusters, our final dataset detected 18,687 CAGE clusters,
161 covering 9,809 GENCODE genes (Figure S2; annotation breakdown) and 826 FANTOM5
162 enhancers. For comparison, we generated corresponding bulk CAGE data using the nAnT-
163 iCAGE method(Murata *et al.*, 2014) for each sample (0, 6, and 24 h, in triplicates) sequenced to
164 median a depth of 10.7M reads.

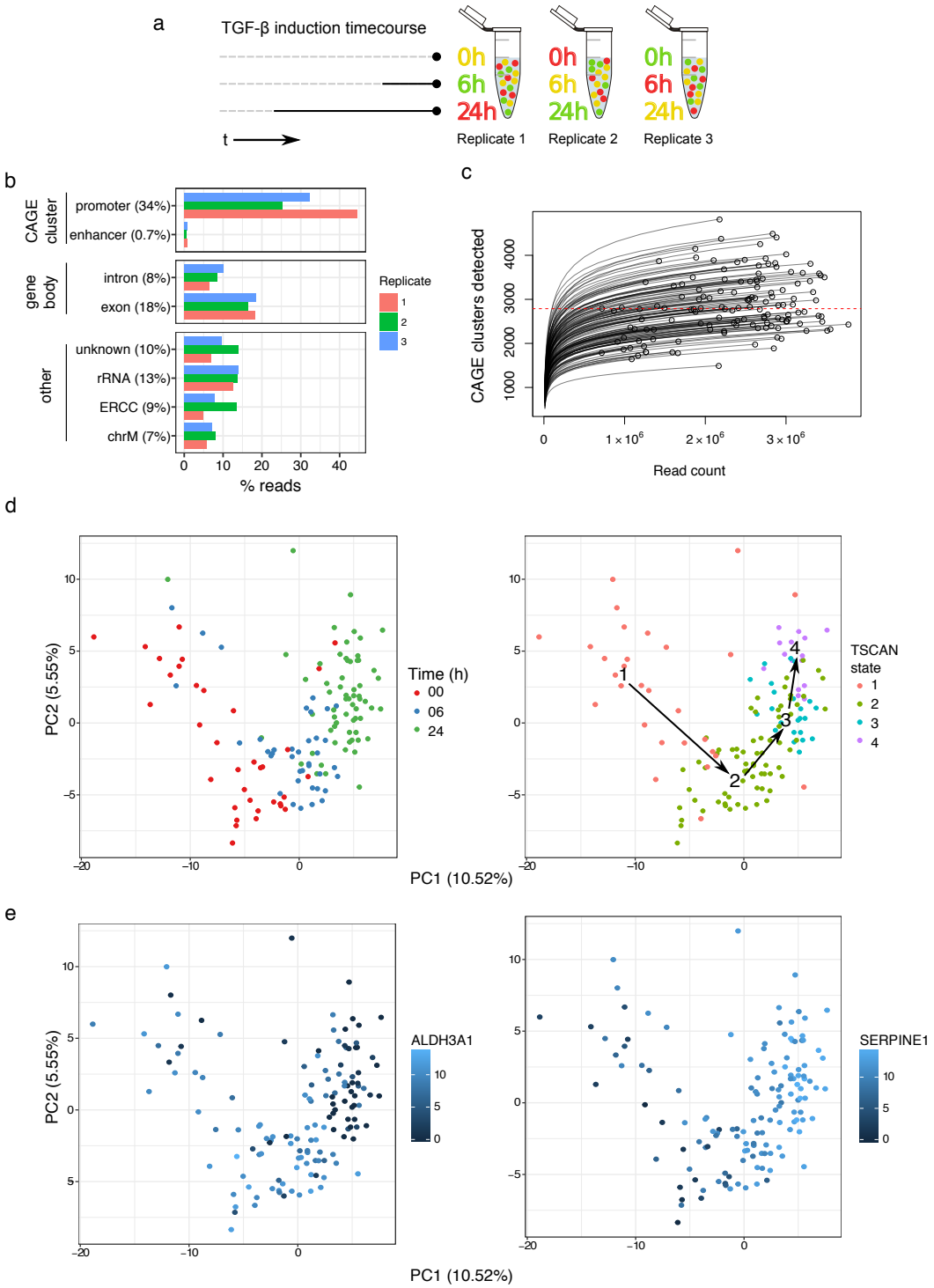

Figure 2: Multiplexing time course strategy

(a) Different color combinations of cells from each time point are added to each replicate. (b) Forward read 5'-end counts by annotation category. Mean read percentage per category shown in brackets. (c) Count of CAGE clusters within each cell after subsampling. Dashed red line at median (2,788). (d) PCA of cells performed on variable subset of CAGE clusters, percentage of

171 variance explained by components shown, cells colored by time point and TSCAN state. (e)
172 PCA of cells performed on variable subset of CAGE clusters, percentage of variance explained
173 by components shown, cells colored by expression values for the marker genes *ALDH3A1* and
174 *SERPINE1* demonstrating that the dynamics of TGF-β response are captured by the TSCAN
175 states.

176 **Dynamic TSS regulation upon TGF-β treatment**

177 To identify TSS that are dynamically regulated during TGF-β treatment, we performed
178 pseudotime analysis on a variable subset of CAGE clusters with TSCAN(Ji and Ji, 2016).
179 TSCAN divided the pseudotime ordering into four distinct states, which showed considerable
180 consistency with the time points, as seen by PCA (Figure 2d). We also confirmed the
181 consistency of the TSCAN states by visualizing the expression levels of two highly variable
182 CAGE clusters for known EMT marker genes, *ALDH3A1* and *SERPINE1*, which showed a clear
183 shift in expression levels from 0 h to 24 h (Figure 2e). To understand the influence of the cell
184 cycle on how TSCAN defined the states, we calculated G2M scores with the cyclone package
185 using the pre-calculated data trained on human embryonic stem cells (hESCs)(Scialdone *et al.*,
186 2015; Leng *et al*., 2015). The clear separation of scores between states 1 and 2 points to the
187 possibility that half (16/35) of 0 h cells were in proliferative states prior to TGF-β stimulation
188 (Figure 2d and Figure S3).
189
190 To identify genes that are co-regulated across the TSCAN states, we performed Weighted Gene
191 Co-Expression Network Analysis (WGCNA)(Langfelder and Horvath, 2008), correlating CAGE
192 cluster expression levels across cells. We identified five co-expressed modules: Suppressed
193 (n=1,041), Weak Responding I (n=825) & II (n=164), Early Responders (n=1,775), and Late
194 Responders (n=2,223). We visualized their trajectories across the pseudotime using eigengene
195 profiles to represent the average behavior and show two CAGE clusters from each module with
196 eigengene correlation coefficient of at least 0.3 with p-value less than 0.1 (Figure 3a, b). The
197 module labels were assigned based on these trajectory visualizations: Suppressed, Early and
198 Late Responders represent those genes that undergo strong expression changes with TGF-β
199 activation, whereas Weak Responding I and II represent those with little or no changes in their
200 transcription.

Figure 3: WGCNA clusters of response to TGFβ

(a) WGCNA results in 5 different modules, 3 of which show clear response behavior to TGF-β (Suppressed, Early Responders, Late Responders). (b) Example CAGE peaks from each module. (c) Top three enriched TF binding profiles in each module. (d) Functional analysis using edgeR's implementation of GOseq. Top over-represented GO terms for biological processes are shown.

212 To understand the biological contexts of these modules, we investigated the enrichment of
213 transcription factor binding motifs (Mathelier *et al.*, 2016, Arenillas *et al.*, 2016) and Gene
214 Ontology (GO) terms in each module. Examining motifs enriched in all modules against a
215 randomly generated GC-matched background, we find that the ETS-related factors are most
216 prominent, such as ETVn, ETSn, ELKn, FLI and NFYx factors (Figure S4). The ETS family of
217 transcription factors is well defined to promote metastasis progression in EMT process(Ell and
218 Kang, 2013).
219
220 Examining each module individually against the combined background of all the other modules
221 (Figure 3c, d) we observe the Suppressed Module enriched in GO terms related to DNA
222 replication and the cell cycle. It has been reported that early after TGF-β treatment, the
223 expression of multiple genes that play key roles in regulating cell cycle progression are
224 suppressed(Schneider, Tarantola and Janshoff, 2011). We observe suppressed expression of
225 *CCNB2* known to interact with the TGF-β pathway in promoting cell cycle arrest(Liu *et al.*, 1999)
226 and of *ALDH3A1* known to affect cell growth in A549 cells(Moreb *et al.*, 2008). We also observe
227 enriched motifs for the cell cycle regulators *LIN54* and *GFI1*(Basu *et al.*, 2009; Sadasivam and
228 DeCaprio, 2013). CAGE clusters in the Suppressed module are more highly expressed in
229 TSCAN state 1, which may represent cells which have not yet fully undergone TGF-β induced
230 G1 arrest as explained above.
231
232 Within the Early Responders and Late Responders modules we observe canonical TGF-β
233 response genes, including *KLF6* known to suppress growth through TGF-β
234 transactivation(Botella *et al.*, 2009) and marker genes for EMT such as *SERPINE1* and *FASN*.
235 TGF-β is one of the key signal transduction pathways leading to EMT and several lines of
236 evidence implicate increased TGF-β signaling as a key effector of EMT in cancer progression
237 and metastasis(Massagué, 2008; Ikushima and Miyazono, 2010; Heldin, Vanlandewijck and
238 Moustakas, 2012). We observed upregulation of mesenchymal marker genes, with a clear
239 increase in *Vimentin* (*VIM*) expression starting during TSCAN state 2, and expression of *N-*
240 *cadherin* (*CDH2*) not detected until TSCAN state 2, and then expressed within a subset of
241 cells(Figure S5).
242
243 Within the Late Responders module we observe enrichment for TFAP2 family transcription
244 factors (TFs) (Figure 3c), suggesting that they might play a role in the late response to TGF-β
245 signaling. We examined their expression profiles in both the single-cell and bulk data, and found

246 *TFAP2C* to have a strong time-dependent expression profile in bulk data, and sporadic
247 expression in TSCAN states 1 and 2 but not in the later states(Figure S6). *TFAP2C* is a known
248 marker gene in breast cancer biology, its loss resulting in increased expression of mesenchymal
249 markers associated with the transition from luminal to basal subtypes(Cyr *et al.*, 2015) and the
250 direct repression of cell cycle regulator *CDKN1A*(Williams *et al.*, 2009; Wong *et al.*, 2012).
251
252 Examining differences between the Early Responders and Late Responders modules, we find
253 GO terms relating to cell adhesion enriched in Early Responders genes, and GO terms related
254 to cell communication and signaling enriched in the Late Responders genes (Figure 3d).
255
256 To further dissect the functional heterogeneity in response to TGF-β, we revisited TSCAN states
257 analysis and explored states 3 and 4 which we observe 24 h post stimulation (Figure 2d). To
258 examine differences between the two states, we performed gene set enrichment analysis
259 amongst CAGE clusters from the Early Responders and Late Responders modules with
260 Camera(Wu and Smyth, 2012) and find a number of gene sets significantly upregulated in
261 TSCAN state 4 including Epithelial to Mesenchymal transition (38 genes, FDR=0.003; full
262 results in Supplementary Table 2). This suggests bi-phasic state in response to TGF-β 24 h post
263 stimulation. Interestingly, a previous study implicated bi-phasic state with more severe
264 morphological changes such as cell-to-cell contacts occurring from 10 to 30 h (Schneider,
265 Tarantola and Janshoff, 2011). Thus, the additional states inferred from the pseudotime analysis
266 reveal the asynchronous progression cells upon TGF-β treatment, which would not have been
267 possible with bulk analyses of the three time points.

268 **eRNA in C1 CAGE**

269 Next we asked whether C1 CAGE can detect the dynamic expression of eRNAs. We and others
270 have reported that bidirectional transcription is associated with enhancer activity(Andersson *et*
271 *al.*, 2014). We observe a similar signature of bidirectional transcription at enhancers detected in
272 pooled C1 CAGE and bulk CAGE data sets (Figure 4a), as well as a similar enrichment of
273 DNase hypersensitivity and H3K27 acetylation, indicating that C1 CAGE unambiguously
274 detected the transcription of eRNAs at these active enhancer regions (Figure 4b). To further
275 examine the bidirectionality of eRNAs at a single-cell level, we selected enhancers with at least
276 10 reads in at least 5 cells to filter for the most widely and strongly detected enhancers and
277 avoid bias due to dropout. For each enhancer, we calculated a bidirectionality score in pooled
278 single-cells ranging from 0 to 1, with 0 being perfectly balanced bidirectional and 1 being

perfectly unidirectional. Examining a set of enhancers (n=32) with balanced transcription, we calculated their bidirectionality score within single-cells, where these enhancers were unidirectionally transcribed (single-cell bidirectionality scores >0.9) (Figure 4c, shown in detail for one enhancer in Figure 4d), indicating that simultaneous transcription of eRNAs from both strands is generally not observed within single-cells.

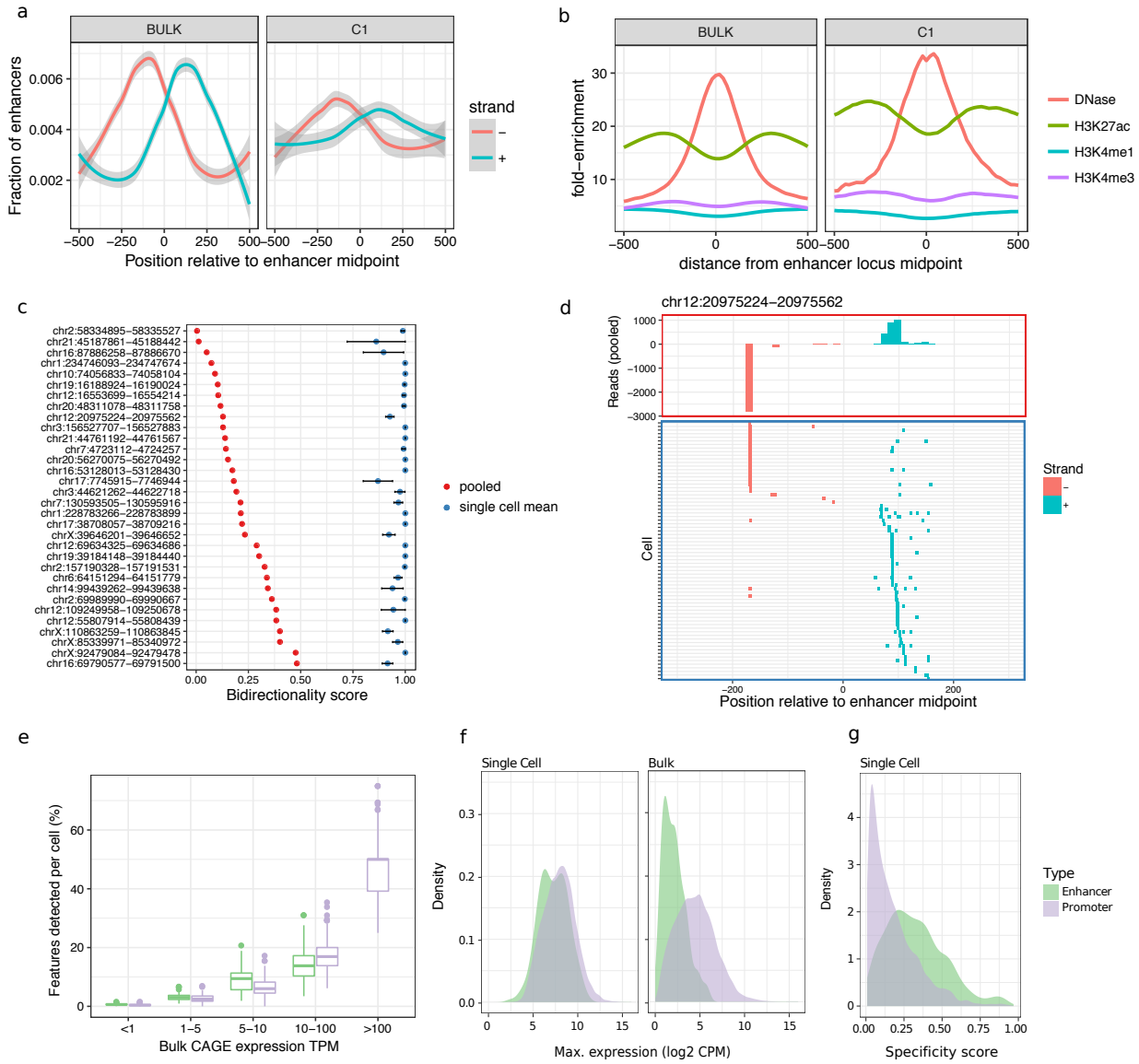

Figure 4: Enhancer analysis at single-cell resolution

Comparison of enhancers detected by bulk CAGE and pooled C1 CAGE data (a) showing bidirectional read profiles smoothed by generalized additive model and (b) epigenetic profiles. (c) Bidirectionality analysis scores (0: equally bidirectional; 1: fully unidirectional) at selected enhancers for pooled cells (red dots) and single-cells (blue dots: mean; black bars: standard

291 error). (d) Example locus on chromosome 12: read profile histogram (upper box), and read
292 presence or absence in single-cells (lower box). (e, f, g) Comparison of enhancers and gene
293 promoters in C1 CAGE and bulk CAGE: (e) Fraction of bulk features detected within each cell,
294 stratified by bulk expression level, (f) Density plots of the maximum expression levels, (g)
295 Specificity score distribution in single-cell data. Lower scores: broad expression (expressed in
296 more cells); higher scores: more specific/enriched expression (fewer cells).
297
298 Although most enhancers were sporadically detected among single-cells, they were detected at
299 a similar level to promoters in single-cells when controlling for expression level (Figure 4e). To
300 assess if enhancers are generally lowly expressed among cells or if they are highly expressed
301 in a subset of cells, we compared the distributions of the maximum expression levels of
302 enhancers and promoters within single-cells and in the bulk data sets (Figure 4f). While the
303 expression of enhancers is generally lower than that of promoters in the bulk data sets, they
304 have similar distributions of expression levels within single-cells. To further evaluate the
305 specificity of enhancer expression in single-cells, we devised a specificity score ranging from 0
306 to 1, with 0 being ubiquitously expressed (i.e. broad expression in many cells), and 1 being
307 specifically expressed (i.e. expression restricted to few cells). We found that enhancers show
308 significantly higher specificity scores than promoters (Figure 4g; Kolmogorov-Smirnov test,
309 D=0.36562, p-value<2.2e-16). This suggests that enhancers behave similarly to promoters
310 which are expressed in transcriptional bursts(Suter *et al.*, 2011; Bahar Halpern *et al.*, 2015) but
311 have fewer numbers of cells where bursts of expression take place, which in turn are averaged
312 out by the total population of cells used to obtain the bulk RNA profile.

313 **FISH validation**

314 To validate the ability of C1 CAGE to detect eRNAs in single-cells, we used smFISH(Femino *et*
315 *al.*, 1998; Raj *et al.*, 2008) to visualize the expression of these transcripts through the TGF-β
316 time course in A549 cells. We first selected intergenic enhancers, filtering out those that
317 overlapped any known transcript models in GENCODEv25, and ranked them by their
318 expression levels. We then searched for their proximal promoters within the same topologically
319 associated domain (TAD) as the potential targets of these enhancers. We selected three
320 enhancers, two of which displayed expression changes across the time-course (Figure S6, S7)
321 and were adjacent to genes known to be involved in TGF-β response, *KLF6* and *PMEPA1*
322 (*KLF6*-eRNA1 at chr10:3929991-3930887 and *PMEPA1*-eRNA1 at chr20:56293544-56293843,

respectively), and a third enhancer (*PDK2*-eRNA1 at chr17:48105016-48105270) adjacent to *PDK2*.

In line with previous reports(Rahman *et al.*, 2016; Shibayama, Fanucchi and Mhlanga, 2017), smFISH for eRNAs gave rise to punctate spots mainly restricted to the nuclei and always no greater than the copy number of the chromosome harboring the enhancer, suggesting that these eRNAs are expressed in low-copy-number and remain at or near their site of transcription. Targeting eRNAs on both strands with the same color, smFISH displayed expression profiles similar to C1 CAGE for the *KLF6*-eRNA1 and *PMEPA1*-eRNA1 enhancers that were upregulated in the C1 CAGE time-course data (Figure 5a, b). In contrast, *PDK2*-eRNA1, whose expression remained steady in smFISH, decreased in the number of cells with signal across the time course in C1 CAGE (Figure S8a).

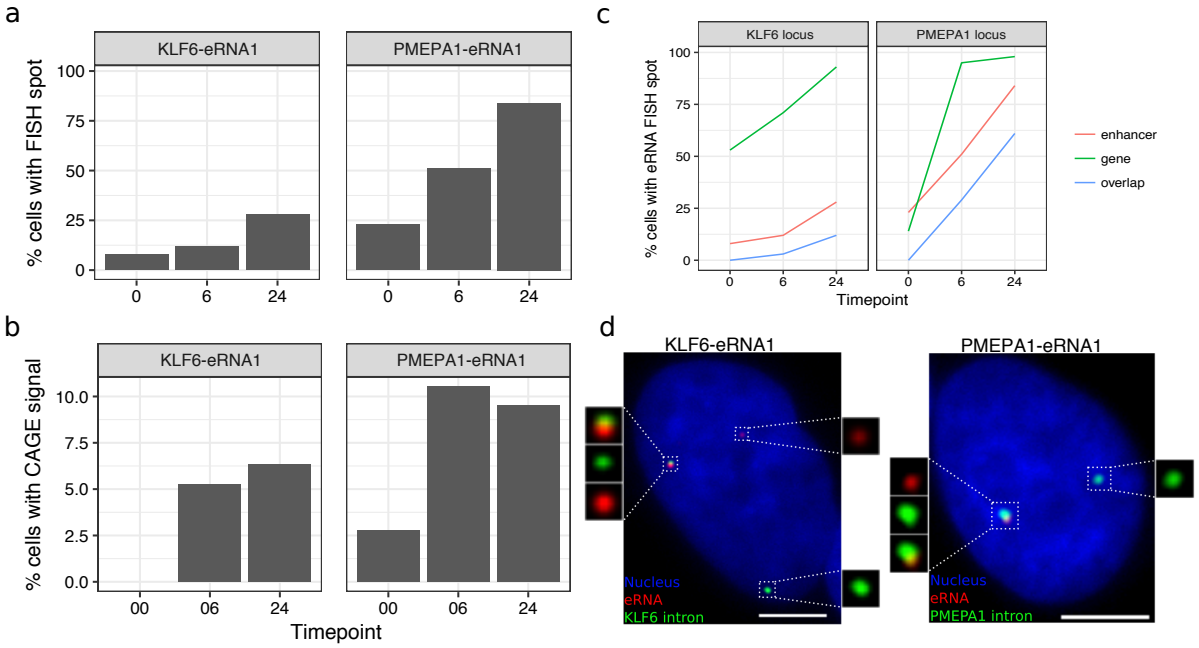

Figure 5: Enhancer and promoter profiles in smFISH

(a, b) Proportion of cells with KLF6-eRNA1 and PMEPA1-eRNA1 detected by (a) FISH, (b) C1 CAGE. (c) Proportion of cells with detected gene intron, enhancer locus and cells with spot overlap at the KLF6 and PMEPA1 loci. (d) Representative images showing gene intron and enhancer locus detection by FISH. Bar = 5 μm. n=100 per time point.

344 For validation of our findings that eRNA were expressed unidirectionally within single-cells, we
345 also targeted the + and – strands of the *KLF6*-eRNA1 and *PMEPA1*-eRNA1 eRNAs in separate
346 colors. In agreement with the C1 CAGE data for these particular enhancers, the majority of the
347 detected spots belonged to eRNAs from only one strand (Figure S8b). In nuclei where eRNAs
348 from both strands were detected, spot co-localization was rare, confirming our suggestion that
349 simultaneous bidirectional transcription of enhancers from single alleles is a rare event.
350
351 Next, we checked for the association of eRNAs with the transcription of nearby genes using
352 smFISH. Visualization of nearby gene transcription was achieved by targeting only the intronic
353 portion (i.e. nascent RNA). Colocalization of an enhancer RNA spot with a nascent RNA spot
354 would suggest the presence of the enhancer RNA at the site of gene transcription, potentially
355 implicating the enhancer's role in promoter activity. Interestingly, nascent transcription of nearby
356 protein coding genes showed similar expression kinetics to the enhancers themselves indicated
357 by increased co-expression of both the protein coding gene and the nearby eRNA in TGF-β
358 stimulated cells (Figure 5c, d, S8c). For KLF6-eRNA1 and PMEPA1-eRNA1, we observed time-
359 dependent increase in colocalization and in the number of nuclei with colocalized spots (Figure
360 5c, d, S9c). In unstimulated cells displaying a basal level of expression of both enhancer and
361 promoter, colocalization of spots could not be observed. This suggests a stimulus-dependent
362 co-activation of enhancer and its association with the nearby promoter. However, a significant
363 portion of transcription sites expressed no enhancer RNA. Possible reasons include a potential
364 delayed interval between transcription events from an enhancer and promoter, during which
365 most enhancer RNA is rapidly degraded. It is also possible that other nearby enhancers may
366 exert their effect on a target promoter. In summary, smFISH could validate enhancer expression,
367 including strand specificity, in single-cells as detected by C1 CAGE.

368 Discussion

369 We examined the response to TGF-β in A549 cells to uncover dynamically regulated promoters
370 and enhancers at single-cell resolution. We highlight enhancer dynamics at single-cell resolution
371 and suggest transcriptional bursting of enhancers, and that while enhancers show bidirectional
372 eRNA transcription in pooled cells, transcripts are generally mutually exclusive.
373
374 Among the eight publicly available transcriptome methods for the C1 platform (Supplemental
375 table 1), only C1 CAGE provides strand-specific whole-transcriptome coverage: its detection of

376 5'-ends is independent from transcript length and polyadenylation owing to the use of random
377 primers. To make the method more accessible, we used a commercially available tagmentation
378 kit in which the transposase is loaded with two different adapters. This adaptation leads to half
379 of the tagmentation products being lost in the process of library preparation. The use of custom
380 loaded transposase, such as in C1 STRT Seq(Islam *et al.*, 2014), would allow reduction of the
381 final PCR amplification by one cycle and enrich extracted reads in the sequencing library,
382 however at the expense of not using standard reagents.
383
384 C1 CAGE has single-nucleotide resolution of transcript 5'-ends, as demonstrated by the data on
385 ERCC spike-ins, where 80% of read one 5'-ends align to the first base. In this study, we did not
386 use ERCC spike-ins for normalization of endogenous genes, preferring to use size factors
387 computed from pools of cells(Lun, Bach and Marioni, 2016), as experimental noise due to spike-
388 in preparation may be introduced(Svensson *et al.*, 2017). Notably, we could detect the ERCC
389 spike-ins even if they are not capped. Nevertheless, C1 CAGE shows a preference for capped
390 ends, as suggested by the fact that the C1 CAGE library contained only 13% reads from
391 ribosomal RNAs. While this range of ribosomal RNA is acceptable, further reduction might be
392 achieved through the use of pseudo-random primers(Arnaud *et al.*, 2016).
393
394 The template-switching oligonucleotides (TSOs) included Unique Molecular Identifier
395 (UMIs)(Islam *et al.*, 2014), however we have not utilized them for molecular counting, because
396 the TSOs carried over from the reverse-transcription could prime the subsequent PCR reaction
397 while tolerating mismatches on the UMI sequence, thus causing a high level of mutation rate (as
398 evidenced by the fact that most UMIs are seen only once). Nevertheless, PCR duplicates are
399 partially removed from our data due to the use of paired-end sequencing, as our alignment
400 workflow collapses the pairs that have exactly the same alignment coordinates. Further
401 improvements of the C1 CAGE might address the mutation rate in UMIs. However, attempts to
402 make the TSOs heat-labile by using full RNA composition have not been successful so far (CP
403 and SK, personal communication).
404
405 Batch effect is a common problem in single-cell RNA-seq, and failing to account for this can
406 lead to cofounding biological interpretations. We introduced, for the first time, an image based
407 approach to decode multiplex samples by using two colors of Calcein AM and their
408 combinations. Moreover, the platform further allows the usage of a larger number of colors or
409 alternatives to Calceins, such as MTT, ATP or MitoBright, which are generally used for live cell

410 monitoring. For instance, we previously used FUCCI fluorescent reporters to detect cell cycle
411 phases(Böttcher *et al.*, 2016). Other potential applications could include the detection of
412 cytoplasmic or nuclear localizations of fluorescent-labelled transcription factors, or cell division
413 counting with fluorescent probes.
414
415 Our cell cycle classification was performed using a model trained on data from H1 hESCs
416 expressing the cell-cycle indicator FUCCI in the C1 system(Leng *et al*., 2015). While training
417 data from phased A549 single-cells would have been preferable, models trained on mouse ESC
418 have also been applied to other cell types with accuracy(Scialdone *et al.*, 2015). However,
419 because the hESC training data was obtained from a 3'-end capture protocol, it may contain
420 different experimental biases that are distinct from our C1 CAGE method. Therefore, these
421 results should be interpreted with caution, and we did not exclude cells based on this
422 classification.
423
424 The chemistry implemented in C1 CAGE–template switching, random priming, and interrogation
425 of 5'-ends–revealed promoter and enhancer activities in lung adenocarcinoma cell line.
426 Enhancers have previously been defined by a signature of balanced bidirectional transcription in
427 bulk data(Andersson *et al.*, 2014). Here we suggest that this signature arises due to generally
428 mutually exclusive transcription from each strand within single-cells. We also suggest for the
429 first time that while eRNAs appear lowly expressed in bulk data, they can be expressed at
430 similar levels to gene promoters within single-cells, although they are expressed in a more
431 restricted subset of cells—i.e. displaying transcriptional bursting.
432
433 Notably, C1 CAGE is not restricted to the use in the C1 platform. Indeed, some of the changes
434 introduced in C1 CAGE are also available for bulk nanoCAGE libraries in our latest
435 update(Poulain *et al.*, 2017). Moreover, the C1 CAGE chemistry might be applicable to profile
436 large numbers of single-cells with droplet based single-cell capture methods. Droplet
437 technologies are more robust to variations of the cell size, and have higher throughput, although
438 they do not allow for the association of imaging. Five-prime-focused atlases will yield greater
439 insights towards promoter and enhancer activities in various biological systems.
440

441 ## Online Methods

442 **Cell culture and TGF-β stimulation**

443 A549 cells (ATCC CCL 185) were grown at 37 °C with 5 % CO_2 in DMEM (Wako, Lot:
444 AWG7009) with 10 % fetal bovine serum (Nichirei Bioscience, Lot 1495557) and
445 penicillin/streptomycin (Wako, Lot 168-23191). At 0 h, 10^6 cells were seeded in 10 cm dishes
446 (TRP, Cat. num. 93100). At 24 h, the medium was replaced with DMEM without serum after 3
447 times washing with PBS (Wako, Lot 045-29795). At 48 h, one third of the dishes were
448 stimulated by treating with 5 ng/ml TGF-β (R&D systems, USA, Accession #P01137). At 66 h,
449 the second third was stimulated with the same treatment. At 72 h, cells for each treatment
450 duration (0 h, 6 h 24 h) were collected and stained with combinations of Calcein AM and Calcein
451 red-orange, (Thermo Fisher Scientific, L3224 and C34851).
452

453 **Cell capture**

454 Calcein stained cells were captured in C1 Single-cell Auto Prep Integrated Fluidic Circuits (IFC)
455 for mRNA Seq, designed for medium-sized (10 to 17 μm) cells (Cat. Num. 100-5760), following
456 manufacturer's instructions (PN 100-7168). In brief, 60 μl of 2.5 × 10^5 cell/ml and 40 μl C1
457 suspension buffer were mixed (all C1 reagents were from Fluidigm), and 20 μl of this mix was
458 loaded into a primed IFC, and processed the script "mRNA Seq: Cell load (1772x/1773x)"
459

460 **Imaging**

461 After loading, IFCs were imaged on INCell Analyzer 6000 (GE Healthcare). Calcein AM was
462 excited at 488 nm and imaged with a FITC fluorescence filter (Semrock). For Calcein red-
463 orange, excitation was at 561 nm (TexasRed; Semrock). Eleven focal planes per chamber and
464 channel were acquired and manually curated to detect empty, dead, singlet, doublet or multiplet
465 cells in the capture site. In case of single-plane imaging, we used the Cellomics platform like in
466 Böttcher et al., 2016[42] (with a green filter (excitation bandwidth: 480-495 nm, emission
467 bandwidth: 510-545 nm), and with a red filter (excitation bandwidth: 565-580 nm, emission
468 bandwidth: 610-670 nm (Thermo Scientific)). Processed and raw single-cell images are
469 available for download from http://single-
470 cell.clst.riken.jp/riken_data/A549_TGF___summary_view.php
471
472
473

474 **Lysis, reverse transcription and PCR for C1-CAGE**

475 Single-cell RNA extraction and cDNA amplification were performed on the C1 IFCs following the
476 C1 CAGE procedure that we deposited in Fluidigm's Script Hub.
477 (https://www.fluidigm.com/c1openapp/scripthub/script/2015-07/c1-cage-1436761405138-3). In
478 brief, cells were loaded in lysis buffer (C1 loading reagent, 0.2 % Triton X, 15.2 U Recombinant
479 Ribonuclease Inhibitor, 37.5 pmol reverse-transcription primer, DNA suspension buffer, ERCC
480 RNA Spike-In Mix I or II (Thermo Fisher, 4456653) diluted either 20,000 times (protocol revision
481 B) or 200 times (revision A)), and lysed by heat (72 °C 3 min, 4 °C 10 min, 25 °C 1 min). First-
482 strand cDNAs were reverse transcribed (22 °C 10 min, 42 °C 90 min, 75 °C 15 min) in C1
483 loading reagent, First Strand buffer, 0.24 pmol dithiothreitol, 15.4 nmol dNTP Mix, betaine, 24.8
484 U Recombinant Ribonuclease Inhibitor, 175 pmol template-switching oligonucleotide, and 490 U
485 SuperScript III. The cDNAs were amplified by PCR (95 °C 1 min, 30 cycles of 95 °C 15 s, 65 °C
486 30 s and 68 °C 6 min, 72 °C 10 min) in a mixture containing C1 loading reagent, PCR water,
487 Advantage2 PCR buffer (not SA), dNTP Mix (10 mM each), 24 pmol PCR primer, 50 ×
488 Advantage2 Polymerase Mix. The PCR products (13 µl) were then harvested in a 96-well plate
489 and quantified with the PicoGreen (Thermo Fisher, P11496) method following the instructions
490 from Fluidigm's C1 mRNA-Seq protocol (PN 100-7168 I1). On-chip cDNA amplification with 30
491 PCR cycles yielded 1.0 ng/µl in average from single cell. A subset of the samples were further
492 controlled by size profiling on the Agilent Bioanalyzer with High Sensitivity DNA Chip.
493

494 **Tagmentation reaction, index PCR and sequence**

495 Amplified cDNAs were diluted to approximately 0.2 ng/µl following the C1 mRNA-Seq protocol,
496 fragmented and barcoded by "tagmentation" using the Nextera XT kit (Illumina, cat. num. FC-
497 131-1096-RN) following the instructions from Fluidigm's C1 mRNA-Seq protocol (PN 100-7168
498 I1), except that we used custom forward PCR primers (dir#501-508/N701-N712, Supplementary
499 Table 3). The final purified library was quality-controlled on a High-Sensitivity DNA Chip and
500 quantified with the KAPA Quantification Kit (Nippon Genetics). Nine pmol were sequenced and
501 demultiplexed on Illumina HiSeq 2500 High output mode (50 nt paired end).
502

503 **CAGE processing**

504 In forward read (Read 1) sequences, linkers were removed and unique molecular identifiers
505 were extracted using TagDust2(Lassmann, 2015). Reverse read (Read 2) sequences were then
506 filtered with the program syncpairs (https://github.com/mmendez12/sync_paired_end_reads) to
507 restore the pairing. The pairs were then filtered against the sequences of the human ribosomal

508 RNA locus (GenBank ID U13369.1), and linker oligonucleotides using TagDust2 v2.13 in paired-
509 end mode. They were then aligned to the human genome version hg19 with Burrows Wheeler
510 Aligner (BWA)'s "sampe" method(Li and Durbin, 2010) with a maximum insert size of 2,000,000.
511 To map the reads on the ERCC spikes at a single nucleotide resolution, we prepared reference
512 sequences of the T7 transcription of the ERCC plasmids, which are now available from the
513 NIST's website (https://www-
514 s.nist.gov/srmors/certificates/documents/SRM2374_putative_T7_products_NoPolyA_v1.fasta)
515 (many RNA-seq studies previously published aligned their reads only to the sequence of the
516 plasmid inserts, which lack transcribed linker sequences, which are essential for aligning CAGE
517 reads precisely to the 5′ ends). The properly aligned pairs were then converted to BED12 format
518 with the program pairedBamToBed12 (https://github.com/Population-
519 Transcriptomics/pairedBamToBed12) with the option "-extraG", and assembled in CAGEscan
520 fragments with the program umicountFP (https://github.com/mmendez12/umicount/). This
521 workflow was implemented in the Moirai system (PMID:24884663) and a prototype implemented
522 in a Jupyter notebook is available on GitHub (https://github.com/Population-Transcriptomics/C1-
523 CAGE-preview/blob/master/OP-WORKFLOW-CAGEscan-short-reads-v2.0.ipynb). The 5′ ends
524 of the CAGEscan fragments represent TSS in the sense of Sequence Ontology's term
525 SO:0000315 ("The first base where RNA polymerase begins to synthesize the RNA transcript").
526
527 **Bulk CAGE**
528 Bulk CAGE data was generated by nAnT-iCAGE method(Murata *et al.*, 2014). Briefly, 5 µg of
529 total RNA prepared from remaining A549 cells after C1 loading. cDNA was reverse transcribed
530 using SuperScript III reverse transcriptase, biotinylated and cap trapped to capture 5' completed
531 cDNAs. Each cDNAs were barcoded and purified. Libraries were sequenced on Illumina HiSeq
532 2500 High output mode (50 nt single read).
533
534 **Image curation and time point demultiplexing**
535 We used the Bioconductor package CONFESS (LOW D and MOTAKIS E (2017). *CONFESS:*
536 *Cell OrderiNg by FluorEScence Signal*. R package version 1.6.0) to detect the cells present in
537 the capture chambers, and quantify the fluorescence in the Green and Red channels. In
538 addition, two curators visually screened the images to confirm the presence of cells, and to
539 detect doublets when focal stacks were available. The final annotation reflects the consensus of
540 the three curations. The results were then cross-checked with other quality control parameters,
541 in particular the amount of cDNAs yielded by the C1 runs, and the fraction of spikes and

542 ribosomal RNA in the libraries. In case of conflicting results, chamber images were re-inspected
543 and re-annotated, if necessary.
544
545 **ERCC spike-in analysis**
546 Accuracy and molecular detection limits were calculated as in Svensson 2017(Svensson *et al.*,
547 2017): The amount of input spike-in molecules for each spike, for each sample, in each
548 experiment was calculated from the final concentration of ERCC spike-in mix in the sample. The
549 calculation of the accuracy of an individual sample was determined with the Pearson correlation
550 between input concentration of the spike-ins and the measured expression values. Molecular
551 detection limit was calculated using the R function glm from the stats package.
552
553 **Read Annotation**
554 The annotation used combined FANTOM5 robust cage clusters for promoters
555 (http://fantom.gsc.riken.jp/5/datafiles/latest/extra/CAGE_peaks/) and enhancers
556 (http://fantom.gsc.riken.jp/5/datafiles/latest/extra/Enhancers/). Promoter clusters were
557 subtracted from enhancer clusters and annotated to their nearest GENCODEv25 within 500 bp
558 where possible. A mask was added to remove rRNA, tRNA, small RNAs, unannotated
559 promoters.
560
561 **Data Processing**
562 After removing low quality cells and multiple single cells captured sites based on imaging data
563 (SCPortalen)(Abugessaisa *et al.*, 2018), the CAGE reads from the remaining 151 cells that
564 overlapped the annotation CAGE clusters were summed together to create the raw counts
565 matrix. This matrix was processed with the scran package(Lun, McCarthy and Marioni, 2016)
566 version 1.6.6 in R 3.4.3 for quality control, filtering and normalization. Following the guideline
567 suggested by the authors of scran, we first removed from our analysis 15 cells with 1) library
568 sizes or feature sizes 3 median absolute deviations (MADs) below their median, or 2)
569 mitochondrial proportion or spike proportion 3 MADs above their median, leaving us with 136
570 cells. All the cells that were dropped due to high spike proportion also had low library sizes and
571 feature counts, whereas this was not necessarily true for those that were dropped due to high
572 mitochondrial proportion. 14 out of the 15 removed cells were from the same C1 run (library 2),
573 but there was no noticeable bias towards any particular time point (5, 3, 7 cells from 0h, 6 h, 24
574 h, respectively). We calculated the cell cycle phase scores using the cyclone method(Scialdone
575 *et al.*, 2015) for each cell. We filtered out low abundance features that were expressed in less

576 than 2 cells or average counts of less than 0.3, leaving us with 18,687 features, of which 826
577 are FANTOM5 enhancers. These features were normalized with size factors calculated based
578 on clusters of cells with minimum size of 30. We then performed mean-variance trend fitting
579 using the whole endogenous feature set, building the sample replicate and Calcein staining
580 variables into the model. We normalized the expression scores to correct for differences of
581 sequencing depth, using a pooling-deconvolution approach(Lun, Bach and Marioni, 2016). We
582 then detrended the data for possible C1 run and Calcein color effects. Lastly, we denoised the
583 data by removing low-rank principal components. To produce the final normalized expression
584 levels for downstream analyses, we reduced the technical noise using scran's denoisePCA
585 function based on the fitted data, then performed batch effect removal with the replicate and the
586 Calcein stain as the covariates using limma package's removeBatchEffect function. We selected
587 high variance CAGE clusters (HVCs) as those with biological variation above the 75% quantile
588 and false discovery rate less than 0.05 after decomposing the total variance for each gene into
589 its biological and technical components using trendVar (scran). We also calculated the pairwise
590 correlations among the HVCs and marked those with FDR greater than 0.05 as significantly
591 correlating HVGs.
592
593 To create the pseudotime ordering with TSCAN (version 1.16.0), we selected the input feature
594 set as the union of the significantly correlating HVCs, the top 100 HVCs and SC3(Kiselev *et al.*,
595 2017) defined marker genes, totaling 290 CAGE clusters.
596
597 **WGCNA**
598 WGCNA version 1.61 was used, with cut height detection threshold of 0.995, minimum module
599 size of 100, signed network type, and merge cut height of 0.25. To reduce noise, we restricted
600 ourselves to those features with mean expression greater than the median of the mean
601 expression across all samples, and biological variation greater than the median. Also, to avoid
602 having the same gene appearing in multiple clusters due to different promoters of the same
603 gene being assigned as such, we only included the major promoter (highest sum of normalized
604 expression across all samples) in the input set, which left us with 6,028 CAGE clusters as the
605 input set.
606
607 **Motif analysis**
608 Motif analysis was performed using CAGEd-oPOSSUM, which employs two separate scoring
609 systems based on JASPAR 2016 transcription factor binding profiles, searching 500bp either

610 side of CAGE clusters: 1) Z-scores, which counts the total number of a given motif found in the
611 input set, and 2) Fisher score, which counts the number of input regions with the given motif.
612 JASPAR motifs with information content greater than 8 bits were searched.
613
614 **Functional analysis**
615 To see if we could identify any functional characteristics of the genes in each module, we
616 performed a test of gene ontology term over-representation test using the edgeR's goana
617 function, which is an implementation of GOseq(Young *et al.*, 2010). For input, we included those
618 CAGE clusters that showed correlation coefficient of greater than 0.2 with p-value less than 0.1
619 with each module's eigengene.
620
621 Camera gene set enrichment analysis(Wu and Smyth, 2012) was performed testing for
622 differential expression between TSCAN states 3 and 4. For the input expression table, we
623 selected the CAGE clusters that were included in the WGCNA analysis and were annotated with
624 Entrezgene IDs. For the test set, we selected those CAGE clusters that showed correlation
625 coefficient of greater than 0.2 with p-value less than 0.1 their module's eigengene from the Early
626 Responders and Late Responders modules. MSigDB Hallmark gene sets were used.(Liberzon
627 *et al*., 2015)
628
629 **TADs**
630 Out of 826 enhancers, 692 could be assigned to a topological association domain (TAD)
631 identified in A549 cells from ENCODE Dataset GSE105600
632
633 **FISH**
634 enhancer RNA lengths were estimated from the ENCODE A549 RNA-seq signal(Dunham *et al.*,
635 2012). We designed oligonucleotide probes consisting of 20 nt targeting sequence using the
636 Stellaris Probe Designer (Biosearch Tech). These sequences were flanked on both ends by 30
637 nt "readout sequence" serving as annealing sites for secondary probes that are labeled with a
638 fluorescent dye(Chen *et al.*, 2015). For each set of probes, all flanking sequences were identical,
639 both on the 5' and 3' ends (Probes listed in Supplementary Table 4). Positive strand eRNA,
640 negative strand eRNA and introns from each locus were assigned different flanking sequences
641 to allow multiplexing. Secondary probes were labeled with either Atto 647 or Cy3 on the 3' end.
642 All probe sequences are listed in supplementary table 4. Briefly, cells were seeded onto
643 coverslips overnight and were fixed in 4% formaldehyde in PBS for 10 min at room temperature.

After fixation, the coverslips were treated twice with ice-cold 0.1% sodium borohydride for 5 min at 4°C. Following three washes in PBS, the coverslips were treated with 0.5% Triton X-100 in PBS for 10 min at room temperature to permeabilize the cells. The coverslips were washed three times in PBS and treated with 70% formamide in 2x SSC for 10 min at room temperature, followed by two washes in ice-cold PBS and another wash in ice-cold 2x SSC. The coverslips were stored at 4°C for no longer than a few hours prior to hybridization. For hybridization, coverslips were incubated in hybridization buffer containing 252 nM primary probes overnight at 37°C inside a humid chamber. Hybridization buffer consisted of 10% formamide, 10% dextran sulfate, 2X SSC, 1µg/µl yeast tRNA, 2mM vanadyl ribonucleoside complex, 0.02% BSA. To remove excess probe, coverslips were washed twice in wash buffer made of 30% formamide, 2x SSC, 0.1% Triton X-100 for 30 min at room temperature and rinsed once in 2x SSC. For hybridization with secondary probes labeled with fluorescent dyes, coverslips were incubated in minimal hybridization buffer (10% formamide, 10% dextran sulfate, 2x SSC) containing 30 nM secondary probes for 3 h at 37°C inside a humid chamber. Coverslips were again washed twice in wash buffer for 30 min at room temperature and rinsed once in 2x SSC. Coverslips were mounted on glass slides using ProLong Gold Antifade Mountant with DAPI (Invitrogen). Imaging was done on a DeltaVision Elite microscope (GE) equipped with a sCMOS camera. Image processing and analysis were done using FIJI.

Enhancer Analysis

For bidirectionality and epigenetic marks analysis a set of enhancers was selected overlapping ReMap(Chèneby *et al.*, 2018) EP300 A549 binding sites. DNase, H3K27ac, H3K4me1 and H3K4me3 bigwig files were downloaded from the NIH roadmap epigenomics project(Roadmap Epigenomics Consortium *et al.*, 2015) and processed with computeMatrix scale-regions from the deeptools package(Ramírez *et al.*, 2016) for enhancer regions. Bidirectional enhancers were selected with at least 10 reads in at least 5 cells and a bidirectionality statistic was calculated as: abs*(plus strand reads - minus strand reads) / sum(reads)* ranging from 0 to 1 with 0 being equally bidirectional and 1 being fully unidirectional. 32 enhancers were selected with absolute score ≤ 0.5. This score was then calculated within each individual cell for these enhancers. The specificity score to indicate how broadly/specifically TSS were expressed we calculated:$Enrichment = Max.Expression \,/\, \sum(Expression\ across\ all\ samples)$.

Data Availability.

C1 CAGE sequence data from this study have been submitted to DDBJ (Project ID: PRJDB5282, Sample ID: SAMD00066188 - SAMD00066475). Alignments were uploaded to the ZENBU genome browser (Severin et al, 2014, PMID 24727769) and a default view is available at http://fantom.gsc.riken.jp/zenbu/gLyphs/#config=NMT9yTLnH59gIVssI9WRfD. In these two submissions the libraries numbered 1, 2 and 3 in this manuscript are numbered 4, 5 and 6, respectively, for historical reasons.

Acknowledgements

This work was supported by a Research Grant from the Japanese Ministry of Education, Culture, Sports, Science and Technology (MEXT) to the RIKEN Center for Life Science Technologies. The authors wish to acknowledge RIKEN GeNAS for the sequencing of the libraries, and Fumi Hori for data deposition to DDBJ.

Author Contributions

Conceptualization: TL, EA, CP, JWS
Ideas; formulation or evolution of overarching research goals and aims.

Data curation: TKo, AK, YH, MM, JSe, IA, CP
Management activities to annotate (produce metadata), scrub data and maintain research data (including software code, where it is necessary for interpreting the data itself) for initial use and later re-use.

Formal analysis: JM, AK, YH, EM
Application of statistical, mathematical, computational, or other formal techniques to analyze or synthesize study data.

Funding acquisition: PC, JWS
Acquisition of the financial support for the project leading to this publication.

Investigation: TKo, YS, SK, MB
Conducting a research and investigation process, specifically performing the experiments, or data/evidence collection.

Methodology: TKo, YS, SK, JL, CP, JWS
Development or design of methodology; creation of models.

Project administration: PC, CP, JWS
Management and coordination responsibility for the research activity planning and execution.

Resources: ST, TA, MF, NR, JW, HS

Provision of study materials, reagents, materials, patients, laboratory samples, animals, instrumentation, computing resources, or other analysis tools.

Software: JM, AK, MB, MM, JSe, IA, AH, TL, CP
Programming, software development, designing computer programs implementation of the computer code and supporting algorithms, testing of existing code components.

Supervision: HS, TKa, TL, CCH, EA, CP, JWS
Oversight and leadership responsibility for the research activity planning and execution, including mentorship external to the core team.

Validation: TKo, YS
Verification, whether as a part of the activity or separate, of the overall replication/reproducibility of results/experiments and other research outputs.

Visualization: JM, AK, IA, CP
Preparation, creation and/or presentation of the published work, specifically visualization/data presentation.

Writing – original draft: TKo, JM, AK, YS, EA, CP, JWS
Preparation, creation and/or presentation of the published work, specifically writing the initial draft (including substantive translation).

Writing – review & editing: JM, CP, JWS
Preparation, creation and/or presentation of the published work by those from the original research group, specifically critical review, commentary or revision– including pre- or post-publication stages.

Conflict of interest

Dr. Ramalingam is an employee and stockholder of Fluidigm Corporation.

752 ## References

753 Abugessaisa, I. *et al.* (2018) 'SCPortalen: human and mouse single-cell centric database.',
754 *Nucleic acids research*, 46(D1), pp. D781–D787. doi: 10.1093/nar/gkx949.
755 Andersson, R. *et al.* (2014) 'An atlas of active enhancers across human cell types and tissues',
756 *Nature*, 507(7493), pp. 455–461. doi: 10.1038/nature12787.
757 Arenillas, D. J. *et al.* (2016) 'CAGEd-oPOSSUM: motif enrichment analysis from CAGE-derived
758 TSSs.', *Bioinformatics (Oxford, England)*, 32(18), pp. 2858–60. doi:
759 10.1093/bioinformatics/btw337.
760 Arnaud, O. *et al.* (2016) 'Targeted reduction of highly abundant transcripts using pseudo-
761 random primers', *BioTechniques*, 60(4), pp. 169–174. doi: 10.2144/000114400.
762 Arner, E. *et al.* (2015) 'Transcribed enhancers lead waves of coordinated transcription in
763 transitioning mammalian cells.', *Science (New York, N.Y.)*, 347(6225), pp. 1010–4. doi:
764 10.1126/science.1259418.
765 Bahar Halpern, K. *et al.* (2015) 'Bursty gene expression in the intact mammalian liver.',
766 *Molecular cell*, 58(1), pp. 147–56. doi: 10.1016/j.molcel.2015.01.027.
767 Basu, S. *et al.* (2009) 'Gfi-1 represses CDKN2B encoding p15INK4B through interaction with
768 Miz-1', *Proceedings of the National Academy of Sciences*, 106(5), pp. 1433–1438. doi:
769 10.1073/pnas.0804863106.
770 Botella, L. M. *et al.* (2009) 'TGF-beta regulates the expression of transcription factor KLF6 and
771 its splice variants and promotes co-operative transactivation of common target genes through a
772 Smad3-Sp1-KLF6 interaction.', *The Biochemical journal*, 419(2), pp. 485–95. doi:
773 10.1042/BJ20081434.
774 Böttcher, M. *et al.* (2016) 'Single-cell transcriptomes of fluorescent, ubiquitination-based cell
775 cycle indicator cells', *bioRxiv*. Available at:
776 http://biorxiv.org/content/early/2016/12/15/088500.abstract.
777 Carninci, P. *et al.* (2006) 'Genome-wide analysis of mammalian promoter architecture and
778 evolution.', *Nature genetics*, 38(6), pp. 626–35. doi: 10.1038/ng1789.
779 Chen, K. H. *et al.* (2015) 'Spatially resolved, highly multiplexed RNA profiling in single cells.',
780 *Science (New York, N.Y.)*, 348(6233), p. aaa6090. doi: 10.1126/science.aaa6090.
781 Chèneby, J. *et al.* (2018) 'ReMap 2018: an updated atlas of regulatory regions from an
782 integrative analysis of DNA-binding ChIP-seq experiments.', *Nucleic acids research*, 46(D1), pp.
783 D267–D275. doi: 10.1093/nar/gkx1092.
784 Cyr, A. R. *et al.* (2015) 'TFAP2C governs the luminal epithelial phenotype in mammary
785 development and carcinogenesis', *Oncogene*, 34(4), pp. 436–444. doi: 10.1038/onc.2013.569.

786 Dunham, I. *et al.* (2012) 'An integrated encyclopedia of DNA elements in the human genome',
787 *Nature*, 489(7414), pp. 57–74. doi: 10.1038/nature11247.
788 Ell, B. and Kang, Y. (2013) 'Transcriptional control of cancer metastasis', *Trends in Cell Biology*.
789 Elsevier Ltd, 23(12), pp. 603–611. doi: 10.1016/j.tcb.2013.06.001.
790 Farh, K. K.-H. *et al.* (2015) 'Genetic and epigenetic fine mapping of causal autoimmune disease
791 variants.', *Nature*, 518(7539), pp. 337–43. doi: 10.1038/nature13835.
792 Femino, A. M. *et al.* (1998) 'Visualization of single RNA transcripts in situ.', *Science (New York,*
793 *N.Y.)*, 280(5363), pp. 585–90. Available at: http://www.ncbi.nlm.nih.gov/pubmed/9554849.
794 Forrest, A. R. R. *et al.* (2014) 'A promoter-level mammalian expression atlas', *Nature*. Nature
795 Publishing Group, 507(7493), pp. 462–470. doi: 10.1038/nature13182.
796 Harrow, J. *et al.* (2012) 'GENCODE: The reference human genome annotation for the ENCODE
797 project', *Genome Research*, 22(9), pp. 1760–1774. doi: 10.1101/gr.135350.111.
798 Hayashi, T. *et al.* (2018) 'Single-cell full-length total RNA sequencing uncovers dynamics of
799 recursive splicing and enhancer RNAs', *Nature Communications*. Springer US, 9(1), p. 619. doi:
800 10.1038/s41467-018-02866-0.
801 Heldin, C. H., Vanlandewijck, M. and Moustakas, A. (2012) 'Regulation of EMT by TGFβ in
802 cancer', *FEBS Letters*, 586(14), pp. 1959–1970. doi: 10.1016/j.febslet.2012.02.037.
803 Hon, C. C. *et al.* (2017) 'An atlas of human long non-coding RNAs with accurate 5′ ends', *Nature*.
804 Nature Publishing Group, 543(7644), pp. 199–204. doi: 10.1038/nature21374.
805 Ikushima, H. and Miyazono, K. (2010) 'TGFbeta signalling: a complex web in cancer
806 progression.', *Nature reviews. Cancer*. Nature Publishing Group, 10(6), pp. 415–24. doi:
807 10.1038/nrc2853.
808 Islam, S. *et al.* (2014) 'Quantitative single-cell RNA-seq with unique molecular identifiers',
809 *Nature Methods*, 11(2), pp. 163–166. doi: 10.1038/nmeth.2772.
810 Ji, Z. and Ji, H. (2016) 'TSCAN: Pseudo-time reconstruction and evaluation in single-cell RNA-
811 seq analysis.', *Nucleic acids research*, 44(13), p. e117. doi: 10.1093/nar/gkw430.
812 Kiselev, V. Y. *et al.* (2017) 'SC3: consensus clustering of single-cell RNA-seq data.', *Nature*
813 *methods*, 14(5), pp. 483–486. doi: 10.1038/nmeth.4236.
814 Lam, M. T. Y. *et al.* (2014) 'Enhancer RNAs and regulated transcriptional programs', *Trends in*
815 *Biochemical Sciences*. Elsevier Ltd, 39(4), pp. 170–182. doi: 10.1016/j.tibs.2014.02.007.
816 Langfelder, P. and Horvath, S. (2008) 'WGCNA: An R package for weighted correlation network
817 analysis', *BMC Bioinformatics*, 9(1), p. 559. doi: 10.1186/1471-2105-9-559.
818 Lassmann, T. (2015) 'TagDust2: a generic method to extract reads from sequencing data.',
819 *BMC bioinformatics*, 16, p. 24. doi: 10.1186/s12859-015-0454-y.

820 Leng, N. *et al*. (2015) 'Oscope identifies oscillatory genes in unsynchronized single-cell RNA-
821 seq experiments.', *Nature methods*, 12(10), pp. 947–950. doi: 10.1038/nmeth.3549.
822 Li, H. and Durbin, R. (2010) 'Fast and accurate long-read alignment with Burrows-Wheeler
823 transform.', *Bioinformatics (Oxford, England)*, 26(5), pp. 589–95. doi:
824 10.1093/bioinformatics/btp698.
825 Li, W., Notani, D. and Rosenfeld, M. G. (2016) 'Enhancers as non-coding RNA transcription
826 units: Recent insights and future perspectives', *Nature Reviews Genetics*. Nature Publishing
827 Group, 17(4), pp. 207–223. doi: 10.1038/nrg.2016.4.
828 Liberzon, A. *et al*. (2015) 'The Molecular Signatures Database (MSigDB) hallmark gene set
829 collection.', *Cell systems*, 1(6), pp. 417–425. doi: 10.1016/j.cels.2015.12.004.
830 Liu, J. H. *et al.* (1999) 'Functional association of TGF-b receptor II with cyclin B', *Oncogene*,
831 18(1), pp. 269–275. doi: 10.1038/sj.onc.1202263.
832 Lun, A. T. L., Bach, K. and Marioni, J. C. (2016) 'Pooling across cells to normalize single-cell
833 RNA sequencing data with many zero counts.', *Genome biology*, 17, p. 75. doi:
834 10.1186/s13059-016-0947-7.
835 Lun, A. T. L., McCarthy, D. J. and Marioni, J. C. (2016) 'A step-by-step workflow for low-level
836 analysis of single-cell RNA-seq data with Bioconductor', *F1000Research*, 5, p. 2122. doi:
837 10.12688/f1000research.9501.2.
838 Massagué, J. (2008) 'TGFβ in Cancer', *Cell*, 134(2), pp. 215–230. doi:
839 10.1016/j.cell.2008.07.001.
840 Mathelier, A. *et al.* (2016) 'JASPAR 2016: a major expansion and update of the open-access
841 database of transcription factor binding profiles.', *Nucleic acids research*, 44(D1), pp. D110-5.
842 doi: 10.1093/nar/gkv1176.
843 Moreb, J. S. *et al.* (2008) 'ALDH isozymes downregulation affects cell growth, cell motility and
844 gene expression in lung cancer cells.', *Molecular cancer*, 7, p. 87. doi: 10.1186/1476-4598-7-87.
845 Mousavi, K. *et al.* (2013) 'eRNAs promote transcription by establishing chromatin accessibility at
846 defined genomic loci.', *Molecular cell*. Elsevier Inc., 51(5), pp. 606–17. doi:
847 10.1016/j.molcel.2013.07.022.
848 Munro, S. A. *et al.* (2014) 'Assessing technical performance in differential gene expression
849 experiments with external spike-in RNA control ratio mixtures.', *Nature communications*, 5, p.
850 5125. doi: 10.1038/ncomms6125.
851 Murata, M. *et al.* (2014) 'Detecting expressed genes using CAGE.', *Methods in molecular*
852 *biology (Clifton, N.J.)*, 1164, pp. 67–85. doi: 10.1007/978-1-4939-0805-9_7.
853 Picelli, S. (2017) 'Single-cell RNA-sequencing: The future of genome biology is now.', *RNA*

854 *biology*, 14(5), pp. 637–650. doi: 10.1080/15476286.2016.1201618.
855 Plessy, C. *et al.* (2010) 'Linking promoters to functional transcripts in small samples with
856 nanoCAGE and CAGEscan', *Nature Methods*, 7(7), pp. 528–534. doi: 10.1038/nmeth.1470.
857 Poulain, S. *et al.* (2017) 'NanoCAGE: A method for the analysis of coding and noncoding 5′-
858 capped transcriptomes', *Methods in Molecular Biology*, 1543, pp. 57–109. doi: 10.1007/978-1-
859 4939-6716-2_4.
860 Rahman, S. *et al.* (2016) 'Single-cell profiling reveals that eRNA accumulation at enhancer-
861 promoter loops is not required to sustain transcription', *Nucleic Acids Research*, 45(6), pp.
862 3017–3030. doi: 10.1093/nar/gkw1220.
863 Raj, A. *et al.* (2008) 'Imaging individual mRNA molecules using multiple singly labeled probes.',
864 *Nature methods*, 5(10), pp. 877–9. doi: 10.1038/nmeth.1253.
865 Ramírez, F. *et al.* (2016) 'deepTools2: a next generation web server for deep-sequencing data
866 analysis', *Nucleic Acids Research*, 44(W1), pp. W160–W165. doi: 10.1093/nar/gkw257.
867 Roadmap Epigenomics Consortium *et al.* (2015) 'Integrative analysis of 111 reference human
868 epigenomes.', *Nature*, 518(7539), pp. 317–30. doi: 10.1038/nature14248.
869 Sadasivam, S. and DeCaprio, J. A. (2013) 'The DREAM complex: Master coordinator of cell
870 cycle-dependent gene expression', *Nature Reviews Cancer*, 13(8), pp. 585–595. doi:
871 10.1038/nrc3556.
872 Schneider, D., Tarantola, M. and Janshoff, A. (2011) 'Dynamics of TGF-β induced epithelial-to-
873 mesenchymal transition monitored by Electric Cell-Substrate Impedance Sensing', *Biochimica*
874 *et Biophysica Acta - Molecular Cell Research*. Elsevier B.V., 1813(12), pp. 2099–2107. doi:
875 10.1016/j.bbamcr.2011.07.016.
876 Scialdone, A. *et al.* (2015) 'Computational assignment of cell-cycle stage from single-cell
877 transcriptome data.', *Methods (San Diego, Calif.)*, 85, pp. 54–61. doi:
878 10.1016/j.ymeth.2015.06.021.
879 Shibayama, Y., Fanucchi, S. and Mhlanga, M. M. (2017) 'Visualization of enhancer-derived
880 noncoding RNA', *Methods in Molecular Biology*, 1468, pp. 19–32. doi: 10.1007/978-1-4939-
881 4035-6_3.
882 Shiraki, T. *et al.* (2003) 'Cap analysis gene expression for high-throughput analysis of
883 transcriptional starting point and identification of promoter usage', *Proceedings of the National*
884 *Academy of Sciences*, 100(26), pp. 15776–15781. doi: 10.1073/pnas.2136655100.
885 Suter, D. M. *et al.* (2011) 'Mammalian genes are transcribed with widely different bursting
886 kinetics.', *Science (New York, N.Y.)*, 332(6028), pp. 472–4. doi: 10.1126/science.1198817.
887 Svensson, V. *et al.* (2017) 'Power analysis of single-cell RNA-sequencing experiments.', *Nature*

methods. Nature Publishing Group, 14(4), pp. 381–387. doi: 10.1038/nmeth.4220.

Tang, D. T. P. *et al.* (2013) 'Suppression of artifacts and barcode bias in high-throughput transcriptome analyses utilizing template switching', *Nucleic Acids Research*, 41(3), p. e44. doi: 10.1093/nar/gks1128.

Trapnell, C. (2015) 'Defining cell types and states with single-cell genomics', *Genome Research*, 25(10), pp. 1491–1498. doi: 10.1101/gr.190595.115.

Tung, P.-Y. *et al.* (2017) 'Batch effects and the effective design of single-cell gene expression studies.', *Scientific reports*. Nature Publishing Group, 7(January), p. 39921. doi: 10.1038/srep39921.

Wagner, A., Regev, A. and Yosef, N. (2016) 'Revealing the vectors of cellular identity with single-cell genomics', *Nature Biotechnology*. Nature Publishing Group, 34(11), pp. 1145–1160. doi: 10.1038/nbt.3711.

Williams, C. M. J. *et al.* (2009) 'AP-2γ promotes proliferation in breast tumour cells by direct repression of the CDKN1A gene', *The EMBO Journal*. Nature Publishing Group, 28(22), pp. 3591–3601. doi: 10.1038/emboj.2009.290.

Wong, P.-P. *et al.* (2012) 'Histone Demethylase KDM5B Collaborates with TFAP2C and Myc To Repress the Cell Cycle Inhibitor p21cip (CDKN1A)', *Molecular and Cellular Biology*, 32(9), pp. 1633–1644. doi: 10.1128/MCB.06373-11.

Wu, A. R. *et al.* (2014) 'Quantitative assessment of single-cell RNA-sequencing methods.', *Nature methods*, 11(1), pp. 41–6. doi: 10.1038/nmeth.2694.

Wu, D. and Smyth, G. K. (2012) 'Camera: a competitive gene set test accounting for inter-gene correlation.', *Nucleic acids research*, 40(17), p. e133. doi: 10.1093/nar/gks461.

Young, M. D. *et al.* (2010) 'Gene ontology analysis for RNA-seq: accounting for selection bias.', *Genome biology*, 11(2), p. R14. doi: 10.1186/gb-2010-11-2-r14.